IFSCC 2025 full paper (IFSCC2025-1074)

"Spontaneous generation of localized ascending and descending flow in the suspension of UV scattering microparticles and Marangoni flow in the applied layer of the suspension and their influence on the structure and UV protecting ability of the deposited layer"

Sakurako Takagi [1], Taisuke Banno [1], Shoji Takekawa [2], Keita Ando [1] and Kouichi Asakura [1,*]

[1] Faculty of Science and Technology, Keio University, Yokohama, Japan; [2] Miyoshi America Inc., Dayville, United States

1. Introduction

Sunscreens are usually composed of volatile solvents, UV scattering microparticles, and UV absorbing oils. Formation of uniform applied layer on the skin is an important factor for their performance. However, Marangoni flow is usually generated during the evaporation process of volatile solvents in the applied layer to deteriorate the uniformity, since the evaporation process makes the applied layer in far-from-equilibrium conditions. Dynamic behavior can be spontaneously generated in far-from-equilibrium conditions to emerge self-organized states, i.e. dissipative structures[1]. Typical examples of such dynamic behavior induced by Marangoni flow are Marangoni contraction[2-4] and tears of wine[5, 6], and they are generated in binary solutions spread on a solid substrate during their evaporation. When the binary solution is the mixture of less volatile solvent possessing lower surface tension and highly volatile solvent possessing higher surface tension, rapid evaporation of highly volatile solvent near the contact line reduce the local surface tension to generate Marangoni flow from the contact line to the center to form dynamic sessile droplets (Figure 1(a)). On the other hand, tears of wine occurs if the binary solution is the mixture of a less

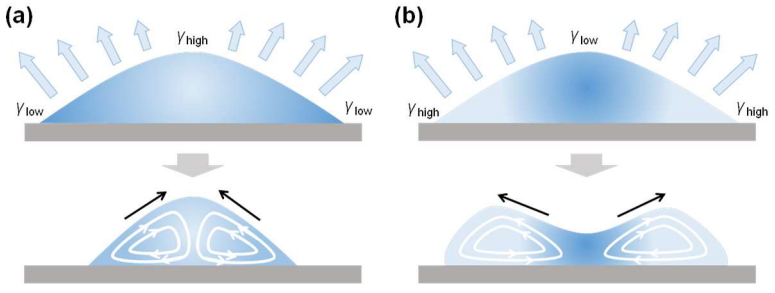

Figure 1. Schematic illustration of dynamic behavior induced by Marangoni flow. (a) Marangoni contraction. Marangoni flow is generated from the contact line to the center to form dynamic sessile drops.; (b) Tears of wine. Marangoni flow from the center to the contact line forms a ridge at the periphery and the droplets are formed by splitting of the ridge.

volatile solvent possessing higher surface tension and a highly volatile solvent possessing lower surface tension. In this case, the highly volatile solvent possessing low surface tension is rapidly evaporated in the vicinity of contact line to make the local surface tension to increase. This causes the Marangoni flow from the center to the contact line to form a ridge at the periphery followed by its splitting into droplets (Figure 1(b)). Generation of these dynamic behaviors in the applied sunscreen layers may vary their structures. In our previous report, UV protecting ability of applied sunscreen layers was found to be strongly influenced by their spatial non-uniformity[7-11]. Therefore, if Marangoni flow is generated in the applied sunscreen layers, it may alter their UV protecting ability.

Spontaneous generation of fluctuated behavior of sedimenting particles[12] may become another factor to influence the structure of sunscreen layers. In a suspension containing glass particles, fluctuated behavior was observed in each particle during their sedimentation[13]. Although the particles are denser than the surrounding liquid, even an upward movement was observed. Observation of this phenomenon indicates that localized ascending flows are generated during the particles sedimentation. It is anticipated that the downward movement of the particle in the gravity field brings the excluded volume of liquid upward direction to induce the localized ascending flow. UV scattering microparticles are usually contained in sunscreens, and their sedimentation behavior in applied sunscreen layers may influence their structures to alter their UV protecting ability. Spontaneous generation of fluctuated behavior is observed not only in particle sedimentation in suspension but also in rising bubbles dispersed in liquids. Collective descending movement of bubbles was observed in Guinness beer[14] and water in which micro bubbles are generated[15]. Although those bubbles are generally expected to rise due to their lower density compared to the surrounding liquid, these studies observed a phenomenon in which bubbles move downward along the inner wall of the vessel.

These scientific backgrounds motivated us to investigate the behavior of applied layer of suspensions in which UV scattering microparticles are dispersed during the liquid evaporation. In this study, suspension samples were prepared by dispersing UV scattering microparticle in a binary solution. In some cases, UV absorbing oil was added to the suspension samples. Behaviors of the applied suspension sample layers were observed during the solvent evaporation process. Structures of the resulting sample layers obtained after the completion of solvent evaporation were analyzed and their UV protecting ability was evaluated. In addition, microparticle sedimentation process in the suspension samples was observed to see whether this system spontaneously generate fluctuated behavior.

2. Materials and Methods

2.1. Preparation of UV scattering microparticle suspension

The UV scattering microparticle employed in this study was a triethoxyoctylsilane treated titanium dioxide (TS), and the solvent was a binary solution of isododecane (ID) and decamethylcyclopentasiloxane (D5) having the volume ratio at 1:1. TS was mixed with the binary solution by setting the weight ratio at 1:3, and the mixture was ground in a bead mill (Easy Nano RMB Ⅱ, Aimex Co. Ltd.) at a rotational speed of 1405 rpm for 45 min. The dispersion thus prepared was diluted with the binary solution to prepare suspension sample, and the weight ratio of TS to the binary solution was set at 1:15. A solution of UV absorbing oil, ethylhexyl methoxycinnamate (EHMC), was prepared by dissolving it in the binary solution, and the concentration of EHMC was set at 1 vol%. Suspension samples containing this UV absorbing oil were prepared by using this solution instead of using the binary solution without containing

EHMC. In this study, the binary solution of ID and D5 having the volume ratio of 1:1 was identified as Sample **1**. The solution prepared by dissolving EHMC into Sample **1** was identified as Sample **2**. The suspension samples prepared by mixing TS with Sample **1** and **2** were identified as Sample **3** and **4**, respectively.

2.2. Application of suspension samples and subsequent observation of the behavior during solvent evaporation

A square quartz plate of one side of 10 cm was cleaned up by corona-discharge treatment for 0.5 min using Laboratory Corona Treater (BD-20AC, Electro-Technic Products). This treatment makes the surface super-hydrophilic[9], and 100 μL of each sample was applied on this substrate using four-sided applicator having four different gaps. Amount of sample applied on the substrate could be controlled by selecting different gaps. Linear motor coater being assembled from a linear motor actuator (LMS-30-C2-L555-5.0, PBA Systems. Pte Ltd.) was employed for the sample application, and the application velocity was set at 3.0 cm s^{-1}. All the application experiments were carried out by setting the temperature of suspension samples at 25 ± 1 °C. In addition, room temperature and the temperature of all the equipment used for the experiment were set at 25 ± 1 °C. Temperature of the experimental equipment, such as the applicator and quartz plate, was measured using an infrared thermography camera (ETS320, FLIR Systems, Inc.) just before the application experiments. Behavior of the applied layer was observed using three types of digital optical microscope (400-CAM057, SANWA SUPPLY INC., DVM6, Leica Microsystems, and BX51TRF, OLYMPUS Corporation) during the solvent evaporation. Size of the dynamic droplets emerged during the solvent evaporation was determined on the recorded images using ImageJ.

2.3. Analyses of the structure of applied sample layers after the completion of solvent evaporation and evaluation of their UV protecting ability

Pictures of the applied sample layer formed after the completion of solvent evaporation were photographed using an iPhone 12 mini (MGAP3J/A, Apple Inc.). Scanning electron microscopy (SEM) observation was conducted on the surface of the resulting applied sample layer using a tabletop SEM (TM3030Plus, Hitachi High-Technologies Corporation). In addition, the spatial distribution of each element was evaluated by scanning electron microscopy-energy dispersive X-ray spectrometry (SEM-EDS) analysis using the same tabletop SEM. UV protecting ability of the applied sample layers was measured using an SPF analyzer (SPF-290AS, Solar Light Company, Inc.).

2.4. Observation of sedimentation behavior in suspension samples

Well mixed Sample **3** and **4** were poured into cylindrical vial tubes (2.8 cm in diameter, 4.5 cm in height), and their tops were capped. After the vial tubes were shaken vigorously, their sedimentation processes were monitored using a video camera (HC-V480MS, Panasonic Corporation) and a digital microscope (400-CAM057, SANWA SUPPLY INC.). Time evolutions of the height of microparticle sedimented layers were determined on the recorded images.

3. Results and Discussion

3.1. Behaviors observed in the applied suspension sample layer during the solvent evaporation and their influence on the structure and UV protecting ability of resulting sample layer

In the case of Sample **1**, many Marangoni contraction droplets were found to be generated in all parts of the applied layer due to the differences in volatility and surface tension

between ID and D5. Then, the coalescence of Marangoni-contraction droplets proceeded to result in the single large droplet disappearing at the completion of evaporation. In the case of Sample **2**, initial behavior was similar to that of Sample **1**. However, in the later stage, most of the ID had been evaporated, and due to the differences in volatility and surface tension between D5 and EHMC, the tears of wine phenomenon occurred. As a result, the single large droplet became flattened before the completion of evaporation. In the case of Sample **3**, many Marangoni contraction droplets were generated in the early stage similar to the experiment using Sample **1**. Migration of microparticle occurred from the center to the periphery of each Marangoni contraction droplet to generate many pores in the microparticle deposited layer. However, no extensive coalescence of Marangoni contraction droplets occurred, and the flow behavior in the later stage scarcely altered the structure of the microparticle deposited layer. Thus, the resulting sample layer possessed numerous fine pores (Figure 2(a)). In the case of Sample **4**, in the later stage of solvent evaporation, around ten coalesced Marangoni contraction droplets became flattened by the tears of wine phenomenon. This Marangoni flow smoothed the surface of the microparticle deposited layer to plug up the pores. Therefore, the large number of small pores generated in the early stage of the solvent evaporation mostly disappeared, and the large ring-shaped pattern in which EHMC was concentrated at each periphery remained at the completion of solvent evaporation (Figure 2(b)).

Experiments for analyzing the relation between the structure and UV protecting ability of the resulting sample layers were conducted by applying Samples **3** and **4** using a four-sided applicator with gaps ranging from 10 to 50 μm. In the case of Sample **3**, significant generation of pores was observed when the gap of the applicator was equal to or larger than 30 μm (Figure 3(a)). UV absorbance was measured for each sample layer. It was found that increasing the gap above 20 μm and thereby the amount of TS applied did not result in a significant increase in UV protecting ability (Figure 4(a)). The results indicated that pores are more likely to be formed by increasing the thickness of the applied layer of Sample **3** and the generations of pores inhibit the enhancement of UV protecting ability although the amount of UV scattering microparticle increases. In contrast, no significant pores were observed in the applied layer of Sample **4** by increasing the gap of applicator (Figure 3(b)), and UV absorbance increased as increasing the gap to 40 μm (Figure 4(b)). Although EHMC is UV absorbing oil, UV absorbance of the applied layers of Sample **3** and **4** was mostly identical with each other when they were prepared by setting the gap of applicator at 10 and 20 μm (Figure 4). The results indicated that

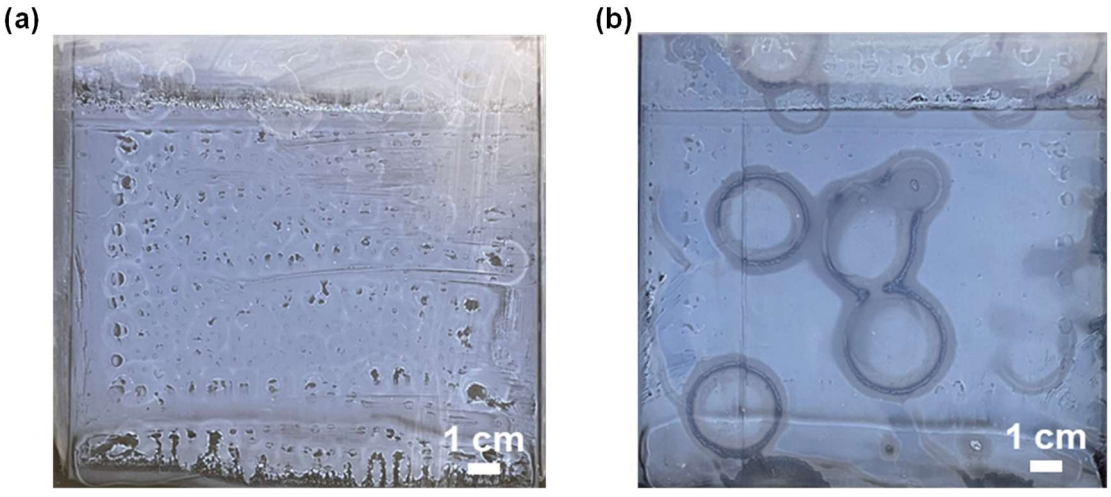

Figure 2. Applied suspension sample layer after the completion of solvent evaporation. (a) Sample **3**; (b) Sample **4**.

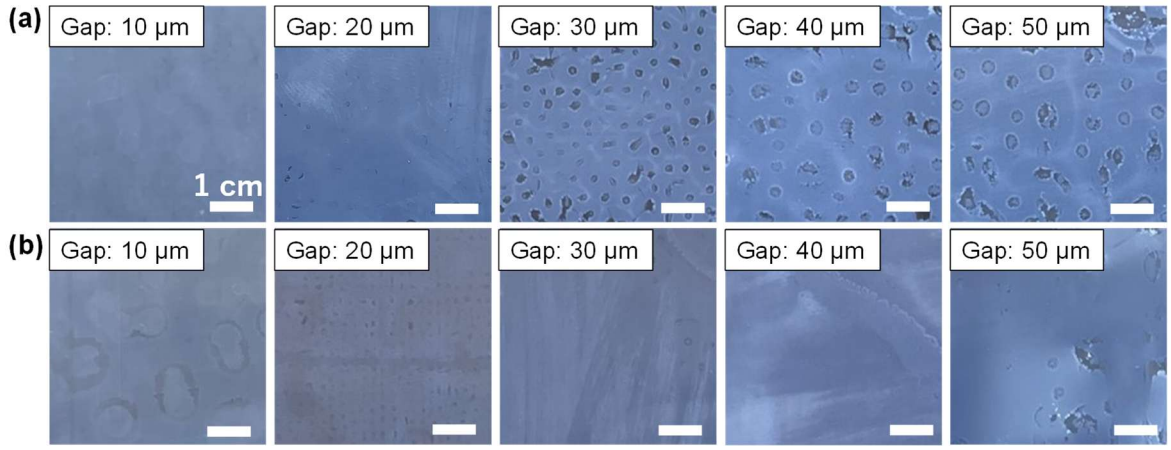

Figure 3. Applied suspension sample layer after the completion of solvent evaporation. Applications were conducted using four-sided applicators with different gap. (a) Sample **3**; (b) Sample **4**.

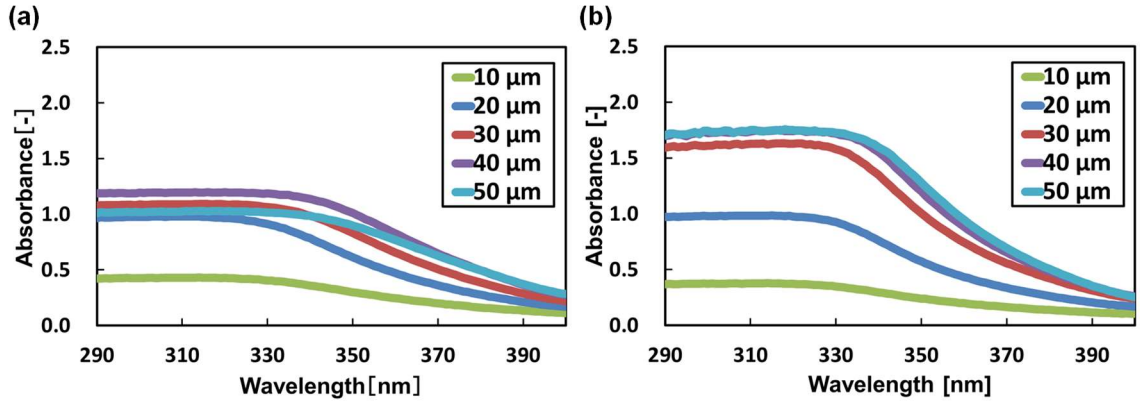

Figure 4. UV protecting ability of the applied sample layers formed using four-sided applicators with different gap. (a) Sample **3**; (b) Sample **4**.

the main reason to enhance the UV protecting ability by the addition of EHMC was not due to UV absorption by EHMC. It was suggested that inhibition of generation of pores in the sample layer by the addition of EHMC enhanced the UV protecting ability.

Behaviors of the dynamic Marangoni contraction droplets were monitored to analyze their influence on the deterioration of the microparticle deposited layer. Sample **1**, **2**, **3**, and **4** were applied using a four-sided applicator with the gap ranging from 10 to 50 μm, and solvent evaporation was allowed to proceed. In the case of Sample **4**, formations of several Marangoni contraction droplets followed by protrusions of donut-shaped ridges at the surrounding region of each initial droplet were observed, and the ridges were split into new dynamic sessile droplets (Figure 5). Similar initial formations of Marangoni contraction droplets followed by protrusions of donut-shaped ridges and their splitting into new dynamic sessile droplets were observed in the applied layer of Sample **1**, **2**, and **3**. The diameter of the initial central droplets was measured, and the average size was calculated. Increasing the applicator gap to increase the thickness of applied layer resulted in larger droplet sizes for all samples (Figure 6(a)), indicating that strength of Marangoni flow was intensified as increasing the thickness of applied layer. By comparing the size of dynamic sessile droplets formed in the applied layer of Sample **1** and **2** and Sample **3** and **4**, it is clear that the presence of TS makes the size of dynamic

sessile drop small. It was considered that the presence of microparticle increased the viscosity of suspension sample to disturb its flow. In the case of Sample **1** and **2** applying by setting the gap of applicator at 40 and 50 μm, distinction of each dynamic sessile droplet whether it was the initial Marangoni contraction droplet or the droplet generated by the splitting of donut-shaped ridge was not possible. In the case of setting the gap of applicator at 20 μm, time evolution of the distance from the initially formed central droplet to the donut-shaped ridge was monitored. It was found that velocity of increasing the distance was significantly retarded in the presence of TS (Figure 6). This result also suggested that strength of Marangoni flow was weakened in the presence of microparticle in the applied sample layer.

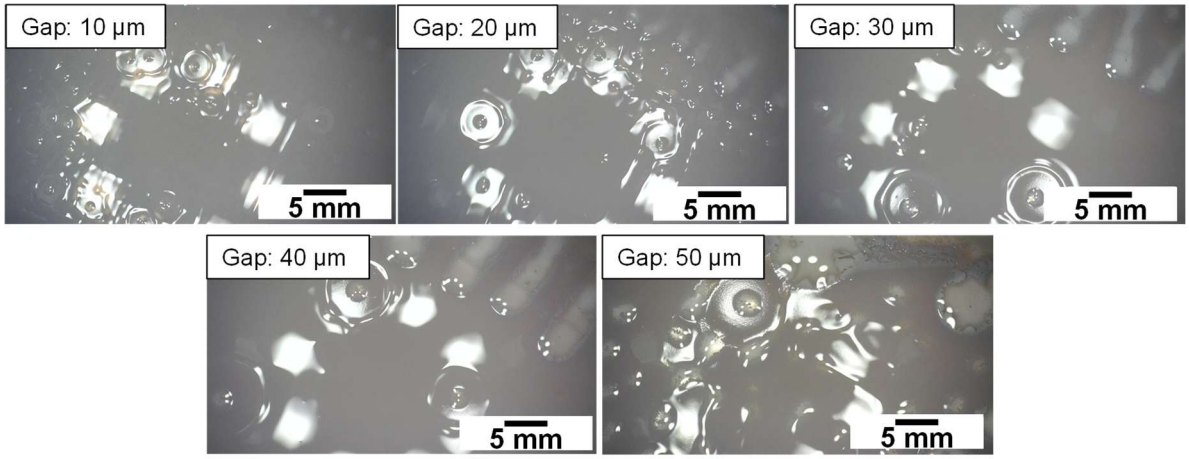

Figure 5. Formations of Marangoni contraction droplets followed by protrusions of donut-shaped ridges at the sorrouding regions of each initial dropletes and splitting of ridges into new dynamic sessile droplets observed during the evaporation process of the applied layer of Sample **4**.

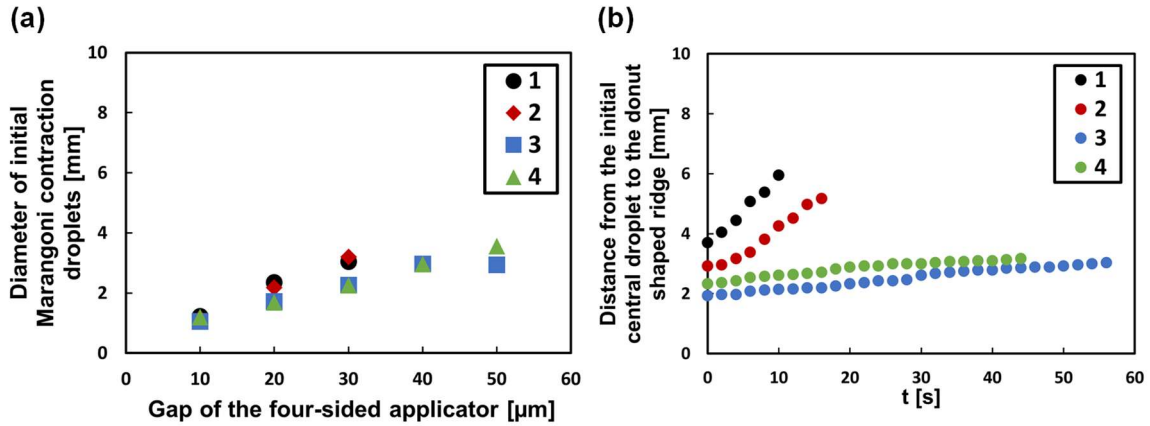

Figure 6. Behavior of Marangoni contraction droplets shortly after the onset of solvent evaporation**.** (a) Relationship between applied layer thickness and average diameter of the initially formed Marangoni-contraction droplets for Sample **1**, **2**, **3**, and **4**; (b) Time evolution of the distance from the initially formed central droplet to the donut-shaped ridge when the gap was 20 μm for Sample **1**, **2**, **3**, and **4**.

3.2. *Surface structure of applied sample layer after the completion of solvent evaporation*

Since many pores were observed in the applied layer of Sample **3** after the completion of solvent evaporation, SEM-EDS analysis was conducted in the vicinity of those pores. Elemental distribution images were obtained for O, Si, C, and Ti (Figure 7). It was shown that Ti was concentrated at the elevated rim of the pore, and UV scattering microparticle TS exclusively consisted of Ti. In addition, there was a region between center and edge of the pores where the amount of Ti was scarce. In the case of Marangoni contraction to arise, Marangoni flow from the periphery to the center is generated at the liquid-air interface, and this leads to generate the reverse direction flow from the center to the periphery at the bottom of the liquid. It was suggested that this reverse flow migrate the microparticles to form this type of spatial distribution in Ti. O and Si were found to be more concentrated in the areas where Ti was scarce, and no clear spatial distribution was observed for C. Ratio of four elements was determined at four locations: i) Center of the pore, ii) Region between center and edge of the pore, iii) Just inside edge of the pore, and iv) Elevated rim of the pore. It was shown that ratio of Ti decreased from the center toward the edge of the pore, however, it exhibited the highest value at the elevated rim. These results confirmed that TS have been transported from the center of the dynamic sessile droplet toward the edge by the flow at the bottom reversed from surface Marangoni flow.

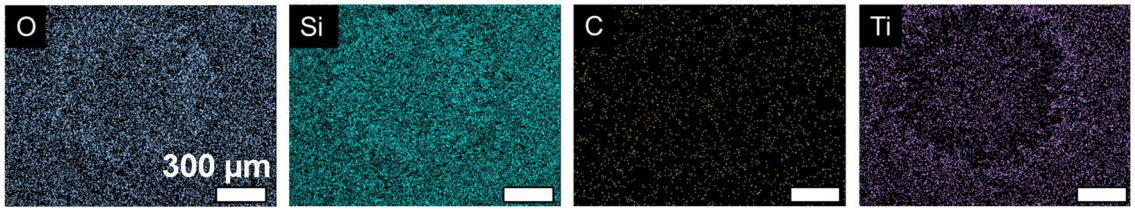

Figure 7. Result of SEM-EDS analysis of the applied layer of Sample **3** after the completion of solvent evaporation.

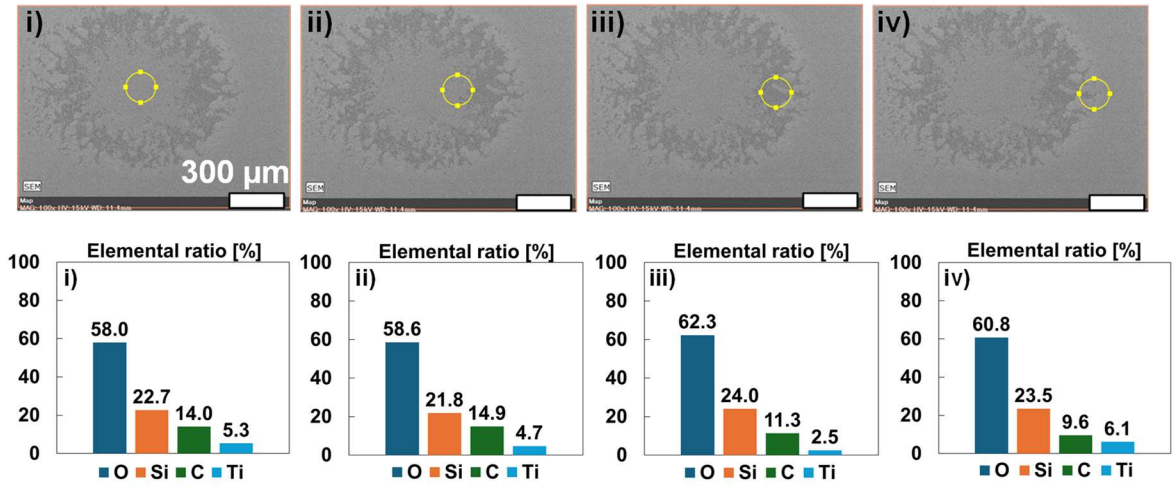

Figure 8. Comparison of ratio of elements at different measurement positions around the pores in the applied layer of Sample **3** after the completion of solvent evaporation. i) Center of the pore; ii) Region between center and edge of the pore; iii) Just inside edge of the pore, and iv) Elevated rim of the pore.

Similar SEM-EDS analysis was conducted on the applied layer of Sample **4** after the completion of solvent evaporation, and the elemental distribution images were obtained for O, Si, C, and Ti (Figure 9). In this case, ring-shaped patterns were remained as shown in the

picture of Figure 2(b) after the completion of solvent evaporation. These are the trace of tears of wine phenomenon occurred in binary solution of D5 and EHMC after the evaporation of ID was mostly completed. SEM-EDS analysis was conducted at the edge of the ring shape pattern. Therefore, strong spatial inhomogeneity in the amount of C was observed, since EHMC was concentrated in this region during the emergence of tears of wine phenomenon. Unlike the applied layer of Sample **3**, pores generated by Marangoni contraction at the early stage of the solvent evaporation were not clearly observed in this case, and this resulted in less spatial inhomogeneity in Ti. Elemental distribution images were obtained for O, Si, C, and Ti in the vicinity of the ring-shaped pattern (Figure 10). Compared to the case of Sample **3**, the ratio of C was higher at all measurement points. However, it shows strong spatial inhomogeneity, with a particularly significant increase in the area where the edge of ring-shaped pattern (Figure 10(a), (b), (c)). Amount of Si in these regions showed considerably small value, indicating that the region was well covered by EHMC.

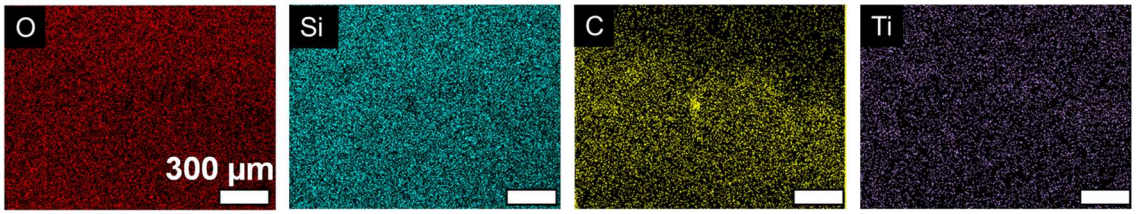

Figure 9. Result of SEM-EDS analysis of the applied layer of Sample **4** after the completion of solvent evaporation.

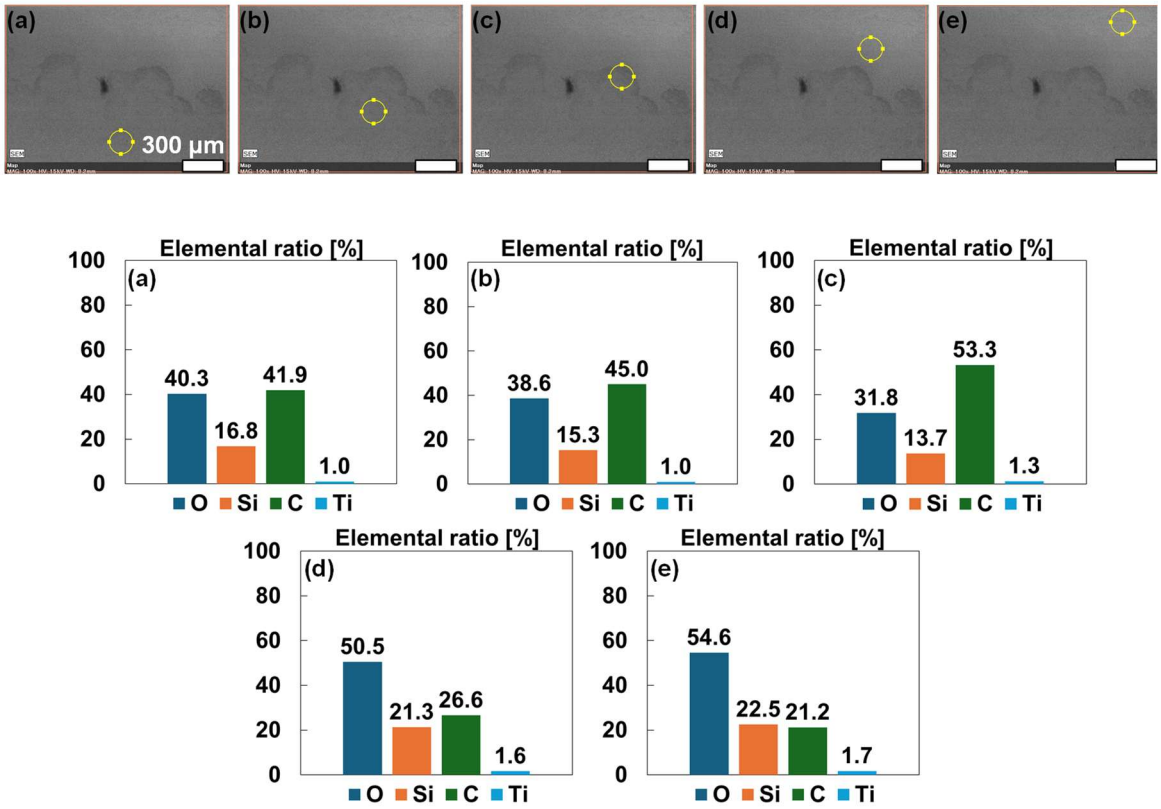

Figure 10. Comparison of ratio of elements at different measurement positions in the vicinity of the ring-shaped pattern in the applied layer of Sample **4** after the completion of solvent evaporation.

3.3. Sedimentation behavior in suspension samples

Sedimentation behaviors of Samples **3** and **4** were observed using a digital microscope (400-CAM057, SANWA SUPPLY INC.). In both suspension samples, nonlinear sedimentation behavior, initial slow sedimentation followed by its acceleration, was observed. Complex flow patterns were found to be generated in both suspension samples (Figure 11), and the onset of acceleration in sedimentation occurred at the same time (Figure 12). Spontaneous generation of the complex flow patterns was the generation of many localized ascending and descending flow. In the case of rising bubbles dispersed in liquids, bubbles forms clouds by sharing each liquid boundary layer of each bubble, and their upward movement in the gravity field bring the excluded volume of liquid downward direction to induce the localized descending flow to lead to the collective local downward movement of clouds of bubbles[14, 15]. In this system, it was suggested that similar phenomenon, i.e. the formation of clusters of TS by sharing liquid boundary layer of each microparticle made their relatively strong downward movement to induce upward flow of excluded volume of liquid. It was anticipated that the resulting many localized ascending and descending flow reduced the viscosity of suspension to accelerate the sedimentation.

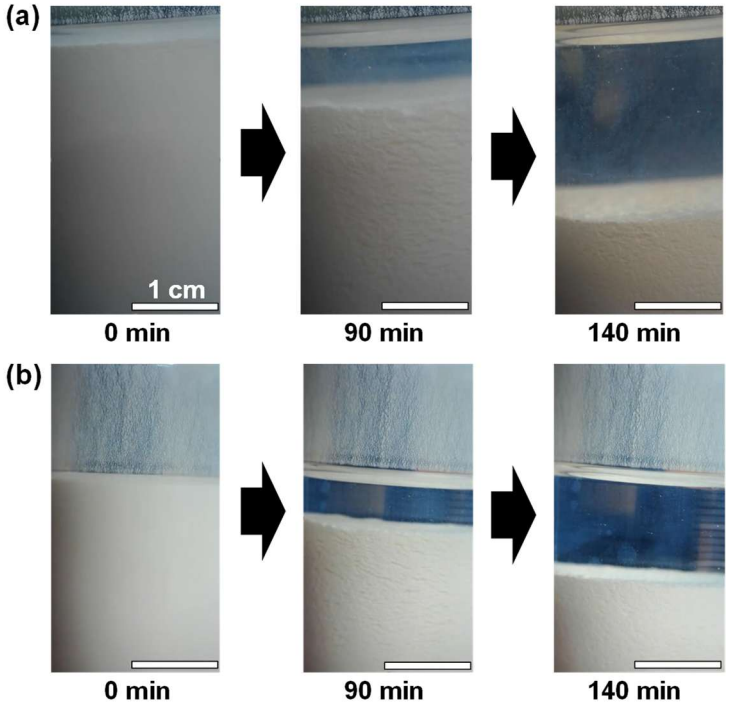

Figure 11. Digital microscope images of suspension samples before, during, and after the onset of acceleration in sedimentation. (a) Sample **3**; (b) Sample **4**.

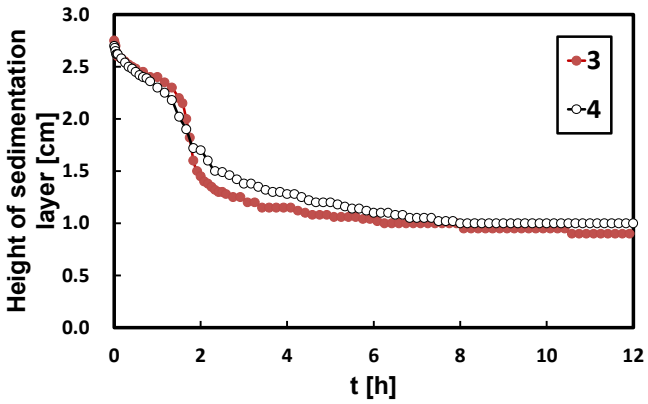

Figure 12. Time evolution in the height of the microparticle sedimented layer in the suspension of Sample **3** and **4**.

4. Conclusion

In this study, attempts were made to analyze the influence of spontaneous generation of flow on the performance of pseudo-sunscreen samples in which surface treated titanium dioxide UV scattering microparticles are dispersed. Binary solution was used as solvent, and

Marangoni flow is usually generated in the evaporation process of binary solution layers. It was found that addition of UV scattering microparticles weakened the strength of Marangoni flow. However, many small pores were generated in their deposited layer as the result of the process called Marangoni contraction during the solvent evaporation from the sample layer. This phenomenon lowered the UV protecting ability of the resulting pseudo-sunscreen layer. Addition of UV absorbing oil, EHMC, was found to smooth the surface of the microparticle deposited layer to plug up the pores by the generation of other Marangoni flow pattern called tears of wine. As the results UV protecting ability significantly increased by the addition of EHMC.

References

1. Kondepudi DK, Prigogine I (1998) Modern thermodynamics: From heat engines to dissipative structures. John Wiley & Sons.
2. Karpitschka S, Liebig F, Riegler H (2017) Marangoni contraction of evaporating sessile droplets of binary mixtures. Langmuir 33:4682-4687.
3. Marra J, Huethorst J (1991) Physical principles of Marangoni drying. Langmuir 7:2748-2755.
4. Hu H, Larson RG (2006) Marangoni effect reverses coffee-ring depositions. J Phys Chem B 110:7090-7094.
5. Fournier JB, Cazabat AM (1992) Tears of wine. Europhys Lett 20:517-522.
6. Shimobayashi SF, Tsudome M, Kurimura T (2018) Suppression of the coffee-ring effect by sugar-assisted depinning of contact line. Sci Rep 8:17769.
7. Fujikake K, Tago S, Plasson R, Nakazawa R, Okano K, Maezawa D, Mukawa T, Kuroda A, Asakura K (2014) Problems of *in vitro* SPF measurements brought about by viscous fingering generated during sunscreen applications. Skin Pharmacol Physiol 27:254-262.
8. Wakabayashi M, Okano K, Mukawa T, Maezawa D, Masaki H, Kuroda A, Asakura K (2016) Problems on the evaluation of the critical wavelength of sunscreens for “Broad Spectrum” approval brought on by viscous fingering during sunscreen application. Photochem Photobiol 92:637-643.
9. Asakura K, Kuroda A (2018) Hydrophilicity of the substrate surface under the applied sunscreen layer changes *in vitro* UV protection efficacies. IFSCC Magazine 21:53-57.
10. Kuroda A, Sakai K, Yahagi S, Mukawa T, Sato N, Nakamura N, Maezawa D, Masaki H, Banno T, Asakura K (2019) Surface structures of cosmetic standard poly methyl methacrylate UV evaluation plates and their influence on the *in vitro* evaluation of UV protection abilities of cosmetic sunscreens. J Oleo Sci 68:175-182.
11. Ikawa K, Aizawa A, Banno T, Fujishiro M, Yahagi S, Kuroda A, Asakura K (2022) New *in vitro* SPF evaluation method for hydrophilic sunscreen samples. J Oleo Sci 71:321-331.
12. Guazzelli É, Hinch J (2011) Fluctuations and instability in sedimentation. Annu Rev Fluid Mech 43:97–116.
13. Guazzelli É (2001) Evolution of particle-velocity correlations in sedimentation. Phys. Fluids 13:1537–40.
14. Watamura T, Iwatsubo F, Sugiyama K, Yamamoto K, Yotsumoto Y, Shiono T (2019) Bubble cascade in Guinness beer is caused by gravity current instability. Sci Rep 9:5718:1–9.
15. Watamura T, Kitagawa A, Murai Y (2019) Cloud structuring of microbubbles ascending along a vertical wall. Chem Eng Sci 208:115121:1-13.